applied sciences

MDPI

Article

Synthetic Rock Analogue for Permeability Studies of Rock Salt with Mudstone

Hongwu Yin [1,2], Hongling Ma [1,2,*], Xiangsheng Chen [1,2], Xilin Shi [1,2,*], Chunhe Yang [1,2], Maurice B. Dusseault [3] and Yuhao Zhang [1,2]

1 State Key Laboratory of Geomechanics and Geotechnical Engineering, Institute of Rock and Soil Mechanics, Chinese Academy of Sciences, Wuhan 430071, China; hong5yin@163.com (H.Y.); bienangua@outlook.com (X.C.); chyang@whrsm.ac.cn (C.Y.); sdkjdxzyh@163.com (Y.Z.)

2 University of Chinese Academy of Sciences, Beijing 100049, China

3 Department of Earth & Environmental Sciences, University of Waterloo, Waterloo, ON N2L 3G1, Canada; mauriced@uwaterloo.ca

* Correspondence: HonglingMa@outlook.com (H.M.); xlshi@whrsm.ac.cn (X.S.); Tel.: +86-027-8719-8721 (H.M.); +86-027-8719-8210 (X.S.)

Received: 28 July 2017; Accepted: 11 September 2017; Published: 14 September 2017

Abstract: Knowledge about the permeability of surrounding rock (salt rock and mudstone interlayer) is an important topic, which acts as a key parameter to characterize the tightness of gas storage. The goal of experiments that test the permeability of gas storage facilities in rock salt is to develop a synthetic analogue to use as a permeability model. To address the permeability of a mudstone/salt layered and mixed rock mass in Jintan, Jiangsu Province, synthetic mixed and layered specimens using the mudstone and the salt were fabricated for permeability testing. Because of the gas "slippage effect", test results are corrected by the Klinkenberg method, and the permeability of specimens is obtained by regression fitting. The results show that the permeability of synthetic pure rock salt is 6.9×10^{-20} m^2, and its porosity is 3.8%. The permeability of synthetic mudstone rock is 2.97×10^{-18} m^2, with a porosity 17.8%. These results are close to those obtained from intact natural specimens. We also find that with the same mudstone content, the permeability of mixed specimens is about 40% higher than for the layered specimens, and with an increase in the mudstone content, the Klinkenberg permeability increases for both types of specimens. The permeability and mudstone content have a strong exponential relationship. When the mudstone content is below 40%, the permeability increases only slightly with mudstone content, whereas above this threshold, the permeability increases rapidly with mudstone content. The results of the study are of use in the assessment of the tightness of natural gas storage facilities in mudstone-rich rock salt formations in China.

Keywords: gas storage; material science; rock permeability; synthetic rock salt testing; Klinkenberg method

1. Introduction

Rock salt possesses characteristics of low porosity, low permeability, reasonable short-term mechanical strength and stiffness and a propensity to creep stably under deviatoric stresses. Rock salt is soluble in water (~1:7 volume ratio for salt and saturated brine), allowing caverns to be dissolved, and salt caverns possess good safety characteristics (environmental and physical security). Studies in the last seven decades have led to commissioning of dissolved salt caverns for the storage of liquids, gases and even solid wastes [1–6]. In several countries (USA, Germany, etc.), salt mines are used to store radioactive wastes. In addition to high safety, dissolved caverns with adequate borehole connections may have large volumetric capacity, fast injection and withdrawal speeds and low operating costs [7].

Underground energy storage (oil, gas, compressed air) has been implemented in very thick salt or salt domes [8]. The USA, Germany, France, Canada and other countries have established underground oil or gas storage, used for commercial short-term or seasonal storage, or as national strategic energy reserves (as in the USA Strategic Petroleum Reserve). Because of the demand for commercial and strategic energy storage, the implementation of large-volume salt cavern underground storage in China has begun.

The key to salt cavern storage security is to ensure the extremely low permeability of the rock salt so as to effectively block the leakage of oil and gas. This is straightforward in thick, clean, deep deposits. However, the rock salt in China we are working with has several characteristics, such as shallow depth, low salt thickness, high impurity content (hard gypsum mudstone, gray mudstone, salt mudstone, sandy mudstone), and so on [9,10]. The physical and mechanical characteristics of these deposits are complex and challenging to measure. Therefore, it is an important design aspect to carefully study the layered rock salt, especially the permeability characteristics, and to develop an understanding using field data and laboratory tests to develop a model.

The permeability characteristics of rock salt have been extensively studied. Field tests show that rock salt permeability is generally less than 10^{-17} m^2 [11,12]. Beauheim and Roberts [13] created a conceptual model for far-field Salado hydrology involved permeability in anhydrite layers and at least some impure halite layers. They note that the pure and most impure salt have negligible permeability because of low porosity and a lack of porosity inter-connection. Their research indicated that in the near-field of an opening in salt rock (excavation damaged zone (EDZ)), dilation, creep and shear can increase the permeability (this should be most severe at layer interfaces between salt and non-salt rocks because of deformation incompatibility). They report typical average permeability values for anhydrite of approximately 10^{-18}~10^{-20} m^2, and for pure halite less than 10^{-20} m^2 [13]. Popp [14] combined gas permeability and P and S wave velocity measurements under hydrostatic and triaxial loading conditions on rock salt specimens from the Gorleben salt dome and the Morsleben salt mine. Isotropic loading markedly decreased permeability, tending toward the in situ matrix permeability (<10^{-20} m^2), with a concomitant wave velocity increase because of progressive closure of grain boundary cracks. The experiments show that permeability change is not only a function of dilatancy, but also of microcrack linkage [14]. Allemandou and Dusseault [15], using before-and-after CAT-scans on 100-mm cores, showed explicit evidence of damage as a thick external annulus of slightly higher porosity (microcracks along grain boundaries), explaining why permeability is so sensitive to isotropic stress in the laboratory. Their results also showed large effects of increased stiffness (>50%) and unconfined compressive strength (>15%) in specimens that had been re-stressed to their in situ stress (annealed) for 72 h. Indeed, sampling damage and slow grain boundary annealing likely account for a substantial amount of the experimental scatter in laboratory measurements of permeability and transient creep in salt and can be taken as evidence that properties are altered in the EDZ in the ground.

In summary, during the investigation of the physical and mechanical properties of interlayers in bedded salt deposits and their effects on storage caverns, it is found that the porosity and permeability of salt and shale are minuscule and of the same order, and values for anhydrite may be somewhat greater. Specimen damage is a significant issue and must be recognized during test programs. In bedded salt storage caverns, anhydrite interlayers may present a greater risk of being a leakage path than shale interlayers for several reasons—creep incompatibility, stiffness and higher intrinsic permeability—so evaluation and testing are needed.

Stormont and Daemen [16] used a pressure pulse method for rock salt with a permeability below 10^{-17} m^2 and found that the permeability within the EDZ is 10^{-16}~10^{-20} m^2, whereas the permeability of intact salt is less than 10^{-21} m^2. Wu et al. [17] tested the permeability of rock salt under different osmotic pressures and compared results using the Klinkenberg effect and the quasi-static pressure method. Yan et al. [18] analysed carbonate strata storage permeability and established relative models for excavation radius, permeability and porosity. Chen et al. [19] used the equivalent boundary gas percolation model to study the gas pressure distribution in the surrounding rock within five years

under different injection pressure conditions in a salt cavern natural gas storage and found that the permeability of bedding surfaces between rock salt and non-salt interlayers has an important influence on the reservoir pressure distribution.

Other similar cases involving materials from salt cavern gas storage core holes have been studied in China to generate models that can allow some generalization of the results. Taking the rock salt underground oil and gas storage facility in Jintan, Jiangsu Province, as a prototype, Zhang et al. [20] developed a reservoir medium geomechanical model for permeability. Ren et al. [21] developed similar materials for cavity experiments, and based on similarity, Jiang et al. [22] developed an artificial model material of rock salt with interlayers.

There are few studies on the permeability characteristics of mudstone-rock salt mixes in the laboratory or in the field, so it is difficult to provide reliable guidance for the construction and maintenance of the pressure integrity for caverns in salt strata with non-salt interlayers. A representative stratigraphy of salt caverns in China is shown in Figure 1.

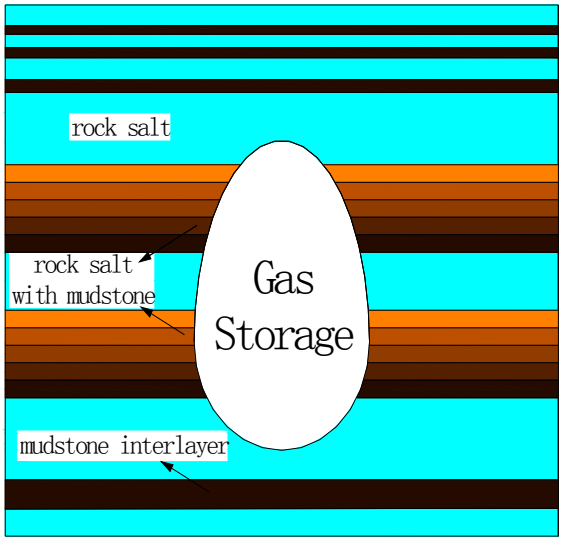

Figure 1. Schematic diagram of a salt cavern gas storage facility.

In this paper, we report on the development of a model material of rock salt with mud and then study and analyze its permeability. We took a storage cavern mudstone interlayer from Jintan and pure rock salt as our basic ingredients and made two kinds of synthetic specimens—mixed and layered—and then carried out permeability tests. These synthetic specimens can be made with any mudstone content, and once a specimen is made, it is straightforward to study the relationships between permeability and mudstone content. Indeed, the permeability testing reveals a reasonably regular relationship between the permeability of rock salt with mudstone and mudstone content, and we then explained the experimental phenomena and results. These results may help provide some methods and guidance for the study of the tightness of layered rock salt gas storage facilities in China.

2. Specimen Preparation

2.1. Material Selection and Specimen Preparation

In order to study the permeation behavior of rock salt with mudstone, we use natural mudstone from the gas storage facility in Jintan from a depth of approximately 934 m–935 m. Relatively pure rock salt is used to develop mud rock/salt specimens with different mudstone content. The intact rock salt has grains that are small and evenly distributed, and the grain boundaries are not strongly apparent. The salt is pale red and has a content of soluble matter over 96.3%.

The weakly consolidated clay forming a strongly consolidated rock through moderate epigenetic effects (such as compaction, dehydration, recrystallization and cementation) is called mudstone. The natural mudstone used in this paper is from the gas storage facility in Jintan from a depth of approximately 934 m–935 m. The mudstone we use is hard, brittle and relatively dense and has some secondary structures such as porous structure, pinhole structure and honeycomb structure in locality. Some of the internal cracks of mudstone are filled by glauberite in a later stage and are stellate distributed. X-ray diffraction shows that quartz, dolomite and illite have the largest proportions in the mudstone, and the average quartz content is about 32%. The mudstone has a small amount of interstitial salt, and the main soluble mineral in the mudstone is glauberite, $Na_2Ca(SO_4)_2$. The XRD result of mudstone is shown in Figure 2.

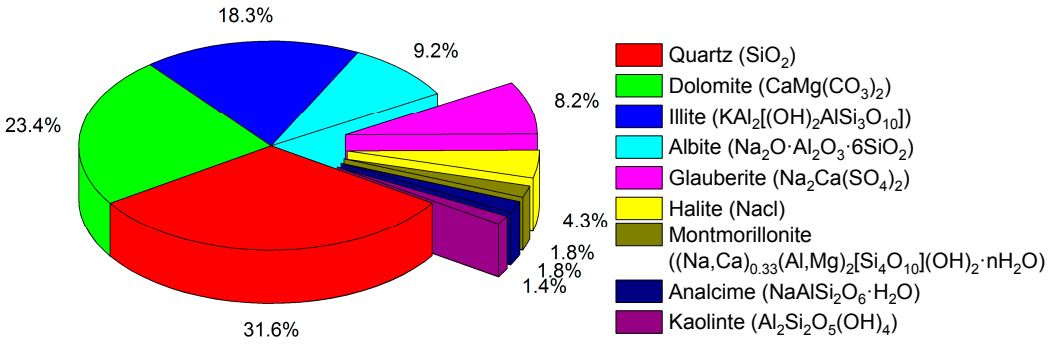

Figure 2. XRD results of mudstone.

The pure rock salt and mudstone (Figure 3) were pulverized into 0.5-mm and 2-mm particles respectively, uniformly mixed with a small amount of cement and near-saturated brine (~1.18 g/cm^3). The pulverized rock salt particles are then placed in a drying box for 24 h, and the mudstone particles are put in a sealed bag.

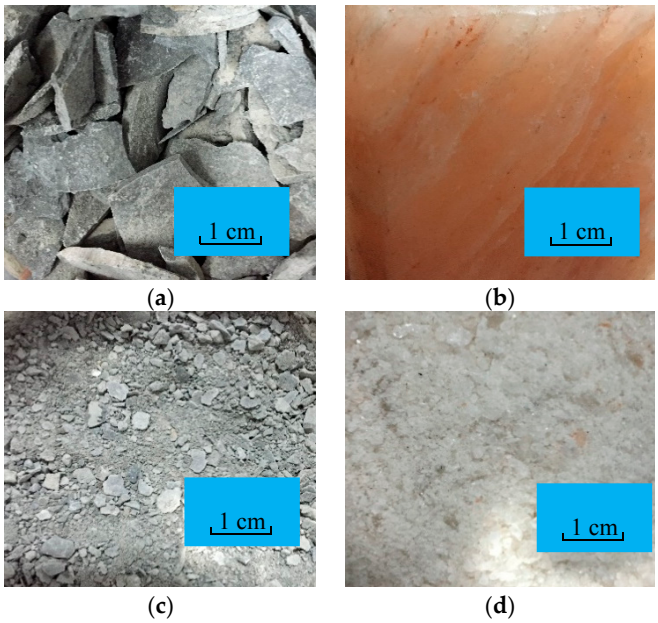

Figure 3. Material selection. (**a**) Mudstone; (**b**) rock salt; (**c**) the particles of mudstone; (**d**) the particles of rock salt.

We make specimens in accordance with the prescribed method [23] with a diameter of 25 mm and an H/D ratio of about two. The rock salt particles and mudstone particles are pressed and formed

by a hydraulic pressure tester, with material proportioning shown in Table 1. Specimens are prepared as follows:

A. Mixed specimens of rock salt with mudstone:

1. Weigh specified amounts of rock salt particles and mudstone particles, as well as cement and brine, then put them in a beaker and stir until homogeneous.
2. Add the mixed material to the pressing mold.
3. Using 120 MPa of compression stress, hold for 2 h.

B. Layered specimens of rock salt with mudstone:

4. Weigh a specified amount of particles of rock salt and mudstone.
5. Place prepared material in the mold in the order of rock salt-mudstone-rock salt.
6. Using 120 MPa of compression stress, hold for 2 h.

Table 1. Material proportions.

Rock Salt with Mudstone	Material Proportion Y:N:C:W
Rock salt	1:0:0:0
Mudstone	0:1:0.12:0.02
Binder	0:0:6:1

Note: Y is the mass of the rock salt; N is the mass of the mudstone; C is the mass of cement; W is the mass of brine.

Note that in nature, the prolonged geological process of compaction takes place under higher temperature, but lower stress for millions of years. In the laboratory, we use ultra-high pressure to yield an artificial specimen with similar porosity to the natural specimens, but of course, there is no time for recrystallization through internal mass transfer.

The specimens are placed in a drying box for 24 h; the physical parameters are obtained, and then, the permeability test is performed. The density of synthetic pure salt is 2.125 g·cm^{-3}, and the density of synthetic pure mudstone is 2.283 g·cm^{-3}, values similar to those from the research of Jiang et al. [22]. The porosity of synthetic pure rock salt is 3.8% with a permeability of 6.93×10^{-20} m^2, and the porosity of synthetic pure mudstone is 17.8% with a permeability of 2.97×10^{-18} m^2. These values are close to those of natural specimens. The two kinds of synthetic specimens are shown in Figure 4, and the physical parameters are listed in Tables 2 and 3.

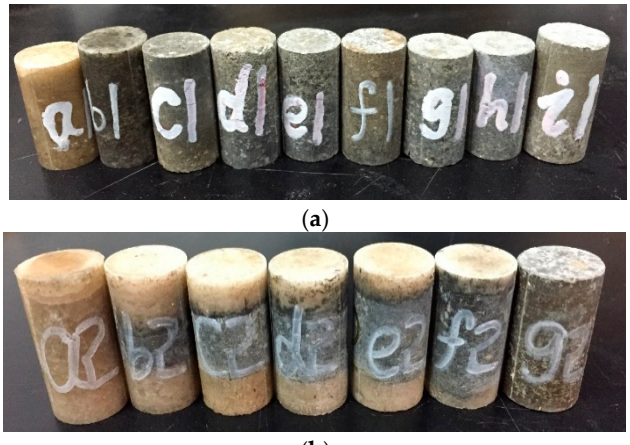

(**a**)

(**b**)

Figure 4. Synthetic specimens. (**a**) Mixed rock salt with mudstone specimens; (**b**) specimens of layered rock salt with mudstone.

Table 2. Physical parameters of mixed specimens.

No.	Diameter (mm)	Height (mm)	Mass (g)	Density (g·cm^{-3})	Mudstone Content (%)
a1	25.47	47.67	51.1576	2.106	0
b1	25.49	52.63	57.1631	2.128	0
c1	25.61	51.17	57.1781	2.169	20
d1	25.57	50.48	57.1842	2.206	40
e1	25.61	49.89	56.9402	2.216	50
f1	25.57	49.23	57.0120	2.255	60
g1	25.69	48.47	56.9275	2.266	80
h1	25.65	47.19	56.9406	2.335	100
i1	25.39	50.01	57.2017	2.259	100

Note: a1 is made of particles of pure rock salt; b1 is synthetic pure rock salt with a small amount of cement and brine; h1 is synthetic pure mudstone with a small amount of cement and brine; i1 is made of particles of pure mudstone.

Table 3. Physical parameters of layered rock salt.

No.	Diameter (mm)	Height (mm)	Mass (g)	Density (g·cm^{-3})	Mudstone Content (%)
a2	25.47	51.49	56.2170	2.143	0
b2	25.63	51.79	57.3667	2.147	20
c2	25.33	50.77	57.4733	2.246	40
d2	25.43	50.62	57.6456	2.242	50
e2	25.39	51.64	59.3861	2.271	60
f2	25.49	49.81	58.5075	2.302	80
g2	25.61	50.08	59.5015	2.307	100

Note: a2 is made of particles of pure rock salt; g2 is made of particles of pure mudstone.

In the preparation process, we find that the compressibility of mudstone is higher than that of rock salt. In Table 3, the mass of a2 is higher than that of g2, but the height relationship is opposite, a reasonable result as the height of the specimen is less with an increase in the proportion of mudstone. The relationship between the specimen height and the mudstone content of b1~h1 is shown in Figure 5.

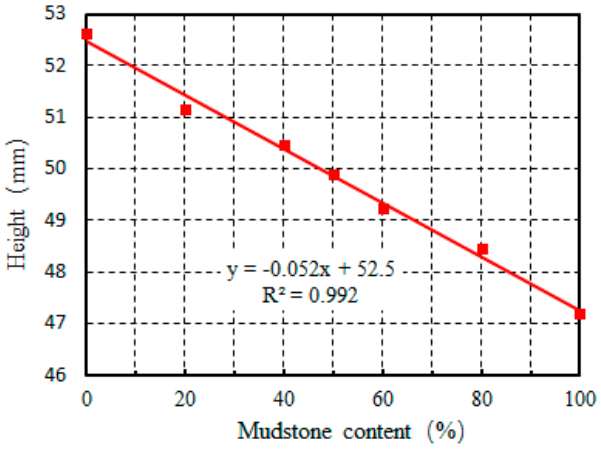

Figure 5. The relationship between the height and the mudstone content of b1~ h1.

2.2. Compressibility Analysis of Mudstone and Rock Salt

From Figure 5, the specimen height variation is linear with the mudstone content under the same mass and stress conditions, and the height of the specimen decreases with the increase of the mudstone content because the mudstone is more compressible than rock salt. The mudstone is porous and composed of clay minerals and other finely divided minerals, so its compressibility is higher than

rock salt. Now, we compare the compressibility of mudstone and rock salt from the theoretical point of view.

Hall [24] defined a rock effective compression factor:

$$c_p = \frac{dV_P}{V_P \cdot dP} \tag{1}$$

where c_p is rock compression factor, V_P is the rock pore volume and P is pressure.

The commonly-used Hall chart curve [25] is shown in Figure 6, and the empirical formula for $c_p - \phi$ is:

$$c_p = \frac{2.59 \times 10^{-4}}{\phi^{0.44}} \tag{2}$$

where ϕ is the porosity of rock.

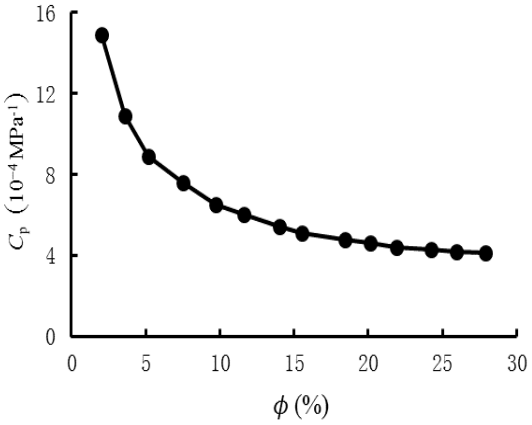

Figure 6. The compressibility × porosity chart from Hall [25].

When the ordinary single-phase solid material is compressed, the compression factor can be defined by the following equation [26]:

$$c_s = \frac{dV_s}{V_s \cdot d\sigma_s} \tag{3}$$

Here, c_s is the compression coefficient of rock solid matter in MPa^{-1}, and σ_s is the average of the three principal stresses of the solid matter in MPa.

In the case of elastic deformation, the compression coefficient for solid matter can be calculated by the following equation [27]:

$$c_s = \frac{3(1-2\nu)}{E_s} \tag{4}$$

where ν is Poisson's ratio and E_s is the Young's modulus. Li [26] derived the following relationship for compressibility and porosity:

$$c_p = \frac{\phi}{1-\phi} c_s \tag{5}$$

For a rock of the same material, c_s is roughly a constant, so the compression coefficient of the rock increases as the porosity increases. At the same time, the mineral properties affect the compression coefficient, and the compression coefficient of the rock decreases as the stiffness of the mineral increases, which is partly why mudstone is easier to compress than salt rock.

3. Permeability Calculation Method

3.1. Klinkenberg Effect

When gas flows in a low permeability porous medium, in contrast to liquid laminar flow, there is a non-zero velocity at the contact with the solid phase, known as gas slippage or the Klinkenberg effect. Gas slippage only occurs when the mean-free-path of the gas molecules and the diameter of the flow channel are comparable, and the lower the rock permeability, the more pronounced the Klinkenberg effect [12,24]. Apparently [12], the mean-free-path of the gas molecules is equivalent to the pore size (10^{-7}~10^{-9} m) of the salt rock when the gas pressure is 0.06~6.00 MPa, and the Klinkenberg effect is significant at this condition, so calibration is needed. Li et al. [28] found that the slippage effect has a great influence on gas seepage when the permeability of a reservoir sandstone is less than 1 mD (millidarcy).

Klinkenberg [29] observed through experiments that in single-phase gas flow through a porous medium, the permeability is:

$$K_g = K_\infty(1 + \frac{b}{\overline{p}}) \tag{6}$$

where K_g is the gas permeability of the rock in millidarcy (mD,1 mD = 10^{-3} μm^2); K_∞ is the absolute permeability (or Klinkenberg permeability) in mD; b is the slip factor (the strength of the slippage effect in the porous medium in MPa); and $\overline{p}$ is the average gas pressure in MPa.

Klinkenberg gave this expression for the slip factor b:

$$b = \frac{4C_1\overline{\lambda}p}{r} \tag{7}$$

where C_1 is a constant (close to one); r is the average radius of the pore in μm; $\overline{\lambda}$ is the mean-free path of gas molecules under average gas pressure, which is given by [30]:

$$\overline{\lambda} = \frac{C_2\mu(\frac{RT}{M})^{\frac{1}{2}}}{p} \tag{8}$$

where C_2 is a constant (close to two); μ is the gas viscosity in mPa·s (10^{-3} Pa·s); R is the universal gas constant (0.86367 L·MPa/(g·mol)); T is the absolute temperature, K; M is the relative molecular weight of the gas.

Substituting Equation (8) into Equation (7):

$$b = \frac{a\mu(\frac{T}{M})^{\frac{1}{2}}}{r} \tag{9}$$

where $a = 4C_1C_2R^{\frac{1}{2}}$.

Clearly, the smaller the pore throat, the higher the value of b [31] and the lower the specimen permeability. The relationship between permeability, porosity and pore throat radius for a circular equivalent pore throat is given by [32,33]:

$$K = \frac{\phi r^2}{8} \tag{10}$$

where K is the liquid permeability in mD, comparable to the Klinkenberg permeability (K_∞); and ϕ is rock porosity.

3.2. Permeability Calculation

The pseudo-pressure method is used to calculate the specimen permeability. The gas seepage equation is based on the following assumptions: (1) the fluid is a one-component gas; (2) the flow is isothermal; (3) the medium is uniform and isotropic, and the porosity ϕ is constant; (4) gravity can be neglected; and (5) flow is laminar so that Darcy's law holds.

Based on the above assumptions and conditions and combining continuity, momentum and state equations, the general form of the partial differential equation for gas seepage is derived [24]:

$$\frac{K_g}{\phi}\nabla\cdot[\frac{p\nabla p}{\mu(p)Z(p)}]=\frac{\partial}{\partial t}[\frac{p}{Z(p)}] \tag{11}$$

Here, p is the gas pressure; Z is the deviation factor for correction of ideal gas; $Z(p)$ is a function of the deviation factor with respect to p; and $\mu(p)$ is the gas viscosity function with respect to p.

The pseudo-pressure is defined as:

$$m(p)=2\int_{p_m}^{p}\frac{p}{\mu Z}dp \tag{12}$$

where $m(p)$ is the pseudo-pressure; p_m is any reference pressure, which can be taken as 0 or 0.1 MPa.

Equations (11) and (12) are used to obtain a partial differential equation, which describes the true gas percolation represented by the pseudo-pressure m.

$$\nabla^2 m=\frac{\phi c_g(p)\mu(p)}{K_g}\cdot\frac{\partial m}{\partial t} \tag{13}$$

where $c_g=\frac{1}{p}-\frac{1}{Z(p)}(\frac{dZ(p)}{dp})_T$ is the isothermal compression coefficient of the real gas.

For an isotropic homogeneous specimen of length L and cross-sectional area A with the pressures at the upper ($x=0$) and the lower ($x=L$) extremes delineated as p_0 and p_L, the seepage equation and the boundary conditions are as follows.

$$\frac{d^2m}{dx^2}=0 \qquad (0<x<L) \tag{14}$$

$$m=m_0=\frac{p_0^2}{\mu_0 Z_0} \qquad (x=0) \tag{15}$$

$$m=m_L=\frac{p_L^2}{\mu_L Z_L} \qquad (x=L) \tag{16}$$

where μ_0 is the gas viscosity at the top of the specimen of length L; μ_L is the gas viscosity at the bottom of the specimen; Z_0 is the deviation factor at the top of the specimen; Z_L is the deviation factor at the bottom of the specimen.

Linear interpolation of (14)–(16) gives:

$$m=m_0-\frac{m_0-m_L}{L}x \tag{17}$$

where x is the distance from the top of the specimen.

Taking the average, $\mu=\mu, Z=\overline{Z}$, we get $m-m_0=\frac{p^2-p_0^2}{\mu\overline{Z}}$. Taking Equation (12) into Equation (17), we can write:

$$p^2=p_0^2-(\frac{\mu\overline{Z}}{\mu_0 Z_0}p_0^2-\frac{\mu\overline{Z}}{\mu_L Z_L}p_L^2)\frac{x}{L} \tag{18}$$

For gas seepage, the volume flow varies with pressure. Using the mass flow F, which is invariant, and assuming that the flow rate is not too large and follows Darcy's law, Kong [24] obtained the volume flow rate Q_{sc} as:

$$Q_{sc} = \frac{F}{\rho_{sc}} = \frac{AK_g T_{sc}}{2pL\mu\overline{Z}T}(p_0^2 - p_L^2) \tag{19}$$

where Q_{sc} is the volume flow rate, ρ_{sc} is the gas density, T_{sc} is the temperature, all under standard conditions, and p is atmospheric pressure.

Equation (19) can also be written as:

$$K_g = \frac{2Q_{sc}pL\mu\overline{Z}T}{AT_{sc}(p_0^2 - p_L^2)} \tag{20}$$

During the test, we keep the outlet pressure constant, change the inlet pressure and get the gas flow rate Q_{sc} at different pressure differences. The gas permeability K_g is obtained according to Equation (20), and the Klinkenberg permeability K_∞ and slip factor b can be determined by fitting the permeability of gas obtained by multipoint measurements through Equation (6).

4. Test Results

4.1. Porosity

4.1.1. Testing Equipment and Principle of Porosity Measurement

Our helium porosity measuring instrument is designed using the standards of the American Petroleum Institute (API) [34] and Geology and Mineral Resources of China to measure the particle volume and helium porosity of rock (Figure 7). The helium atom has the advantages of small volume (minimal viscosity), stable ideal gas behavior and low adsorbtivity on clay mineral surfaces; this gives easy and accurate measurements without altering the nature of the specimen, which is why He measurements are standard in such cases.

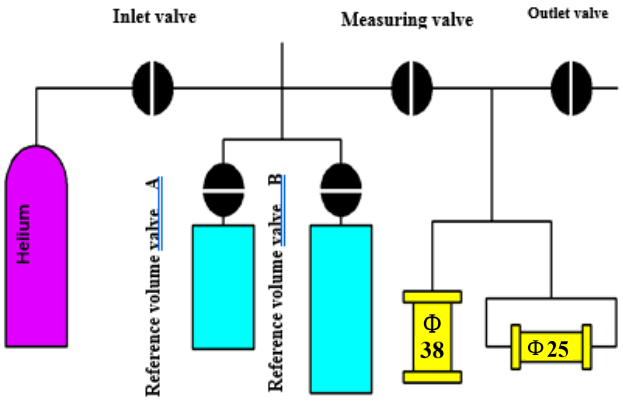

Figure 7. Helium porosity measurement instrument diagram.

Measurement of core porosity by the gas uses Boyle's law:

$$P_1 \cdot V_1 = P_2 \cdot V_2 \tag{21}$$

The porosity is calculated as follows:

$$\phi = \frac{V_P}{V_P + V_G} \times 100\% \tag{22}$$

where ϕ is porosity, V_P is the pore volume, and V_G is the particle volume. The formulae for measuring the particle volume and pore volume are:

$$P_1 \cdot V_R = P_2 \cdot (V_R + V_M - V_G) \tag{23}$$

$$P_1 \cdot V_R = P_2 \cdot (V_P + V_D + V_R) \tag{24}$$

where P_1 is the initial pressure, P_2 is the equilibrium pressure, V_R is the reference volume, V_M is the volume of the media cup, V_D is the volume of the closed system, V_G is the solids volume of the specimen and V_P is the pore volume of the specimen.

Taking Equations (22) and (23) into Equation (21), the porosity is determined. Table 4 displays the porosity test results.

Table 4. The results of the porosity test.

No.	Type	Mudstone Content (%)	Particle Volume (cm^3)	Pore Volume (cm^3)	Porosity (%)
a1	Mixed	0	23.35	1.21	4.9
b1	Mixed	0	26.07	0.79	2.9
c1	Mixed	20	24.66	1.69	6.4
d1	Mixed	40	23.75	3.22	11.9
e1	Mixed	50	23.02	2.67	10.4
f1	Mixed	60	23.51	2.43	9.4
g1	Mixed	80	21.69	3.47	13.8
h1	Mixed	100	20.53	3.95	16.1
i1	Mixed	100	21.39	5.11	19.3
a2	Layered	0	26.11	0.70	2.6
b2	Layered	20	24.89	1.77	6.6
c2	Layered	40	23.83	1.71	6.7
d2	Layered	50	23.65	1.99	7.8
e2	Layered	60	23.79	2.34	9.0
f2	Layered	80	22.66	2.77	10.9
g2	Layered	100	21.56	4.23	16.4

4.1.2. Porosity Test Results

From Table 4, the porosity of synthetic pure rock salt is 3.9%, and the porosity of synthetic pure mudstone is 17.8%. The test results are consistent with the range of natural rock porosity, indicating that our method of using such materials to make similar specimens is reasonable, under the circumstances (no analogue is perfect in geomaterials). The porosity and compressibility of the specimen increase with the mudstone content, which is consistent with the results described in Section 2.2.

4.2. Permeability Test

4.2.1. Test Equipment and Principles

The instrument used for the test is a low permeability measurement instrument designed using the standards of the American Petroleum Institute (API) [34] and Geology and Mineral Resources of China (Figures 8 and 9). It measures the permeability of the rock specimen under steady nitrogen (N_2) gas flow. Changing the upstream pressure, the Klinkenberg permeability and slip factor b can be fitted by the permeability of gas obtained by multipoint measurements.

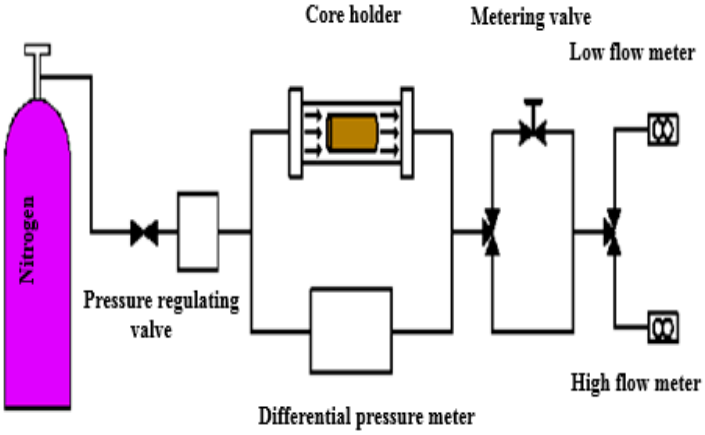

Figure 8. The diagram of the low permeability measurement instrument.

Figure 9. Low permeability measurement instrument.

4.2.2. Permeability Test Results

The permeability of the specimen at different inlet pressures can be calculated by Equation (20). In the experiment, p is the atmospheric pressure, and μ is the viscosity coefficient corresponding to the test temperature. The experimental process is isothermal, and the deviation factor Z is one [24] for N_2 at these conditions, so Equation (20) can be written as:

$$K_g = \frac{2QpL\mu}{A(p_0^2 - p_L^2)} \tag{25}$$

where Q is the test measured volume flow; p is the atmospheric pressure; μ is the viscosity coefficient corresponding to the test temperature; p_0 is the inlet pressure; p_L is the outlet pressure; L refers is the height of the specimen.

Gas flow is perpendicular to the direction of the mudstone salt interface for layered rock salt. During the test, the confining pressure is 1.38 MPa, the outlet pressure 0.10 MPa and the temperature 25 °C. Table 5 shows the results for synthetic pure rock salt Specimens a1, a2 and synthetic pure mudstone Specimens i1, g2.

Table 5. Permeability test results.

NO.	Inlet Pressure (MPa)	Reciprocal of Mean Pressure $1/p$ (MPa^{-1})	Volume Flow ($mL \cdot s^{-1}$)	K_g (10^{-21} m^2)
a1	0.333	4.74	0.008	2.65×10^2
a1	0.414	4.15	0.011	2.29×10^2
a1	0.475	3.62	0.014	2.18×10^2
a1	0.545	3.19	0.017	1.99×10^2
a2	0.305	4.92	0.004	1.75×10^2
a2	0.383	4.13	0.006	1.60×10^2
a2	0.450	3.63	0.008	1.51×10^2
a2	0.523	3.23	0.010	1.38×10^2
i1	0.311	4.84	0.109	4.43×10^3
i1	0.377	4.18	0.158	4.20×10^3
i1	0.451	3.62	0.226	4.11×10^3
i1	0.511	3.27	0.283	3.96×10^3
g2	0.322	4.77	0.093	3.49×10^3
g2	0.388	4.09	0.137	3.43×10^3
g2	0.457	3.58	0.189	3.34×10^3
g2	0.518	3.23	0.242	3.30×10^3

The volume flow rate increases with the increase of the inlet pressure, while the permeability decreases gradually. This indicates that the slippage effect is obvious and consistent with the results of Cosenza et al. [12].

5. Analysis of Test Results

5.1. Comparison of Porosity and Permeability between Synthetic Specimens and Natural Specimens

With Equation (20), we obtained the specimen gas permeability at four different inlet pressures, and the Klinkenberg permeability and slip factor b can be determined by the pseudo-pressure method. The results are shown in Figure 10; the indicators a1~i1 in the figure are mixed specimens of mudstone and rock salt, and Specimens a2~g2 are layered rock salt.

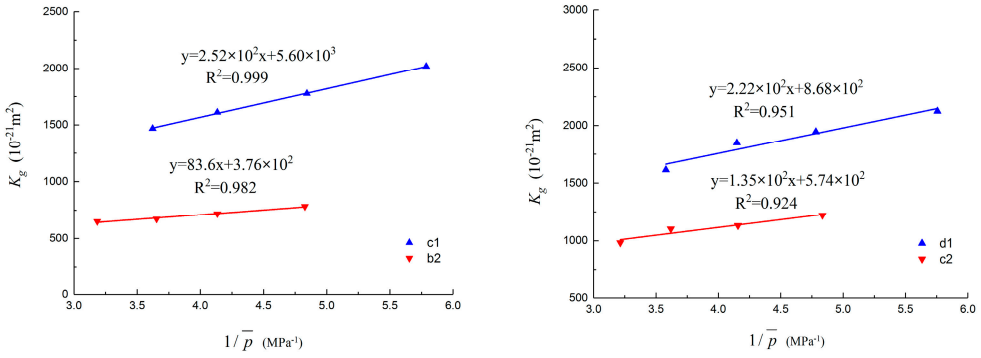

Figure 10. *Cont.*

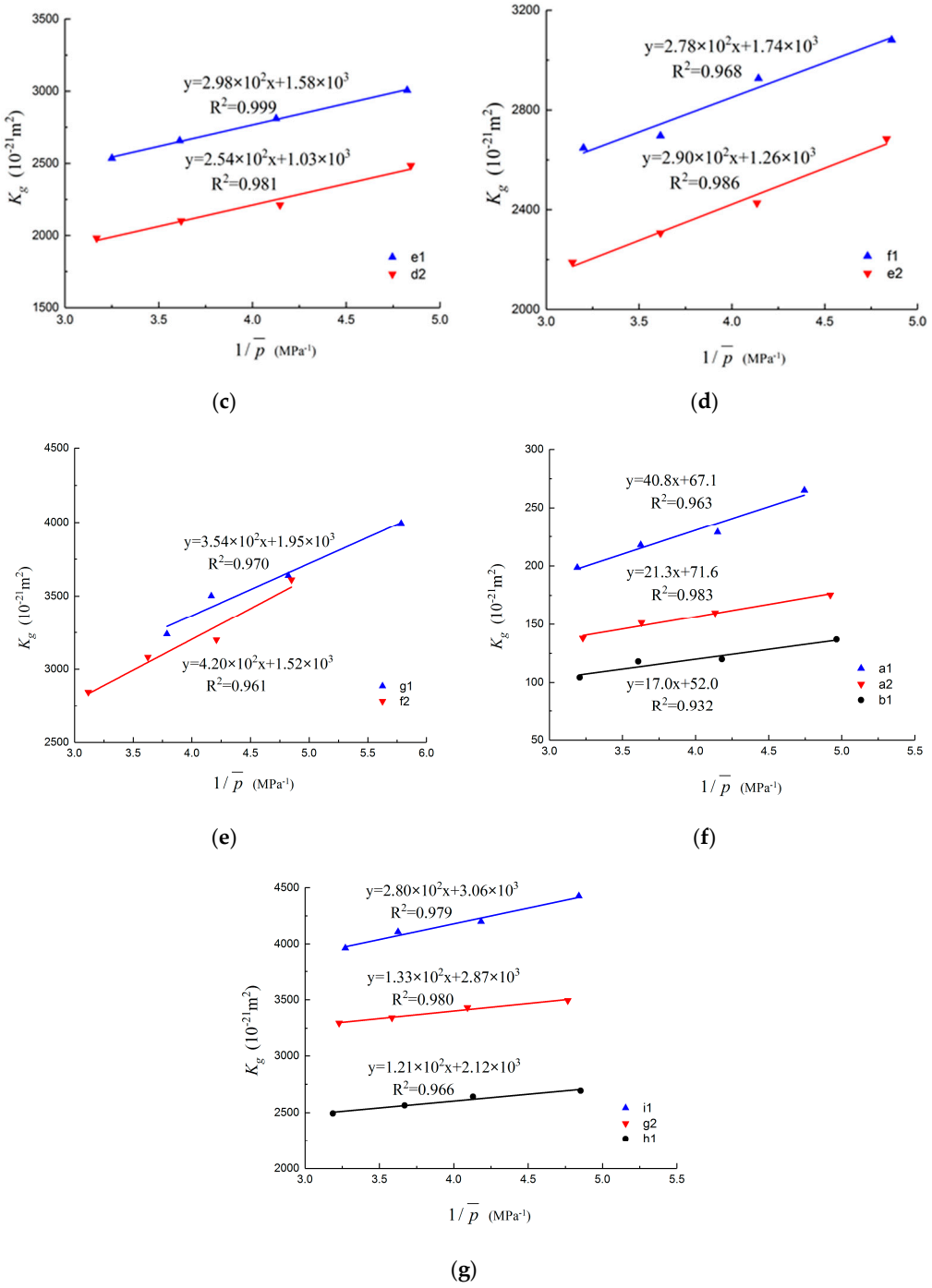

Figure 10. Fitting results of K_g and $1/p$. (**a**) Mudstone content is 20%; (**b**) mudstone content is 40%; (**c**) mudstone content is 50%; (**d**) mudstone content is 60%; (**e**) mudstone content is 80%; (**f**) synthetic pure rock salt and synthetic pure rock salt with binder; (**g**) synthetic pure mudstone and synthetic pure mudstone with binder.

From Figure 10, we can see that the correlation coefficients are close to one, so the results are consistent and reliable. From the data, the Klinkenberg permeability of synthetic pure rock salt specimens is 6.93×10^{-20} m^2 (the average values of a1 and a2), and that of synthetic pure mudstone specimens is 2.97×10^{-18} m^2 (the average values of i1 and g2). The test results are in agreement with the natural specimens, indicating that the model material is a reasonable analogue of the natural material. At the same time, the permeability of synthetic pure rock salt with a small amount of cement

and brine (b1) is about 1/3 lower than that of synthetic pure rock salt, and the permeability of synthetic pure mudstone with a small amount of cement and brine (h1) is about 1/3 lower than that of synthetic pure mudstone. The cement and brine in the mudstone and rock salt particles play a role in blocking permeable channels.

According to the porosity in Table 3 and the Klinkenberg permeability in Table 6, the effective pore throat radius of the synthetic pure rock salt is 1.445×10^{-3} μm calculated by Equation (10) (the average values of a1 and a2), and the effective pore throat radius of the synthetic pure mudstone is 2.059×10^{-2} μm (the average values of i1 and g2). From the comparison of the two kinds of specimens in Figure 10, the results show that the permeability of the mixed specimens is about 40% higher than that of the layered mudstone/salt specimens. In a salt cavern gas facility, the permeability of the transition zone of rock salt and mudstone is likely to be higher than that of layered mudstone/salt interbed area. The permeability of the rock salt bands in situ is of course very low because the crystals are large, the grain arrangement is dense and the pore throat equivalent radius is small. Yang [35] found that the interface of rock salt and mudstone is not weak, and the rock salt crystals and mudstone particles form a zig-zag interface. Because the intact rock salt permeability is low, the interface of the rock salt with the mudstone plays a leading role in overall permeability. Note that the equivalent pore throat size of mixed specimens formed by two kinds of particles is larger than that of layered rock salt, so the permeability of the mixed specimens is slightly higher than the layered rock salt. The fitting results of Klinkenberg permeability are shown in Table 6.

Table 6. The fitting results.

No.	K_∞ (10^{-21} m^2)	b (MPa)	R^2
a1	67.1	0.61	0.963
b1	52.0	0.33	0.932
c1	5.60×10^2	0.45	0.999
d1	8.68×10^2	0.26	0.951
e1	1.58×10^3	0.19	0.999
f1	1.74×10^3	0.17	0.968
g1	1.95×10^3	0.19	0.970
h1	2.12×10^3	0.06	0.966
i1	3.06×10^3	0.09	0.979
a2	71.6	0.30	0.983
b2	3.76×10^2	0.22	0.982
c2	5.74×10^2	0.24	0.924
d2	1.03×10^3	0.29	0.981
e2	1.26×10^3	0.23	0.986
f2	1.52×10^3	0.28	0.961
g2	2.87×10^3	0.05	0.980

We tested the porosity and permeability of natural specimens in order to compare with synthetic specimens. The porosity of natural pure rock salt is 3.1%, and the porosity of synthetic pure mudstone is 16.9%. The porosity of synthetic pure rock salt is 3.8%, and the porosity of synthetic pure mudstone is 17.8%. The porosity results show that the synthetic specimen porosity is in good agreement with the natural specimen. The picture of the natural specimens and the permeability results can be seen in Figures 11 and 12.

Figure 11. Natuural specimens.

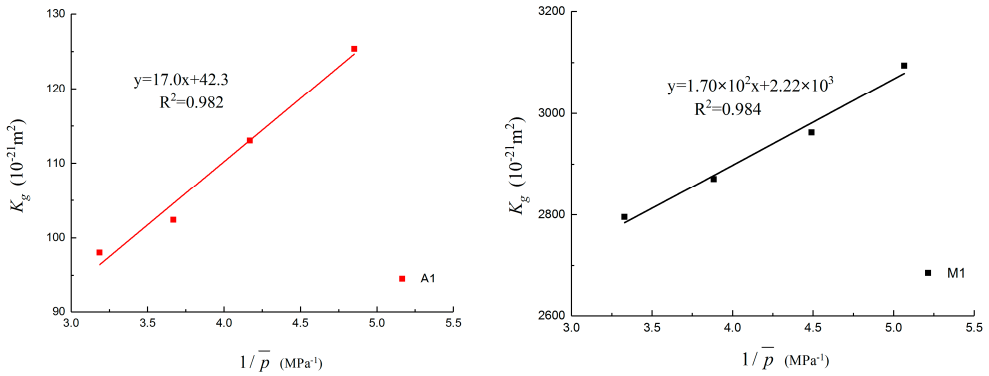

Figure 12. Natural specimen permeability results. (**a**) Natural pure rock salt; (**b**) natural pure rock salt. Note: We define the salt rock with high salt content as pure salt rock (>95%, both for the natural rock salt and synthetic rock salt).

From Figure 12 and Table 7, we can see that the permeability of natural pure salt rock is 4.23×10^{-20} m^2, and the permeability of natural mudstone is 2.22×10^{-18} m^2. From Figure 10, we know that the permeability of synthetic pure salt rock is 6.93×10^{-20} m^2, and the permeability of synthetic mudstone is 2.97×10^{-18} m^2. The permeability results show that the synthetic specimens are in good agreement with the natural specimen.

Table 7. The porosity and permeability of the synthetic specimens and natural rock specimens.

No.	Specimen/Specimen Type	Porosity (%)	K_∞ (10^{-21} m^2)
a1	Synthetic pure rock salt	4.9	67.1
a2	Synthetic pure rock salt	2.6	71.6
A1	Natural pure rock salt	3.1	42.3
i1	Synthetic pure mudstone	19.3	3.06×10^3
g2	Synthetic pure mudstone	16.4	2.87×10^3
M1	Natural pure mudstone	16.9	2.22×10^3

The test results of porosity and permeability of synthetic specimens are close to the natural specimens, which shows that the synthetic material model for permeability testing is a reasonable analogue for the ranges we addressed to emulate the natural cavern conditions.

5.2. Pore Size Distribution of Synthetic Specimens and Natural Specimens

In order to examine the difference between synthetic specimens and natural specimens, we carried out scanning-electron microscope assessment of the synthetic pure rock salt, synthetic pure mudstone, natural pure rock salt and natural pure mudstone. Some images are shown in Figure 13.

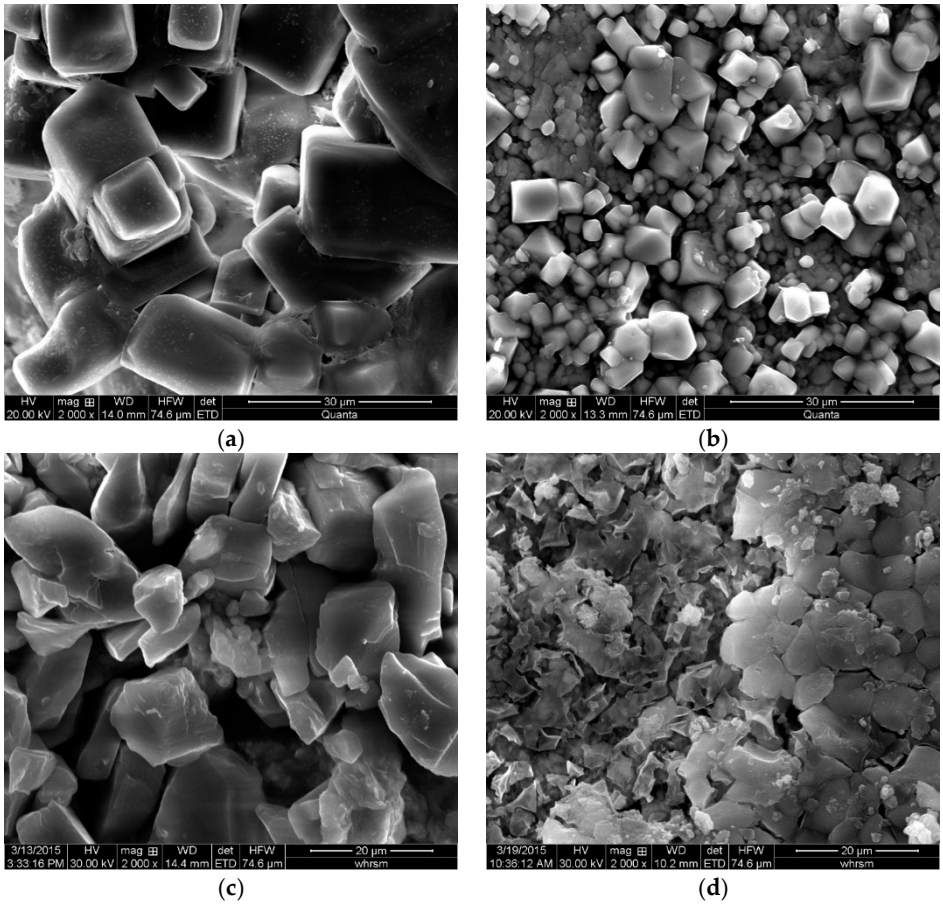

Figure 13. SEM pictures (2000 times). (**a**) Natural pure rock salt; (**b**) synthetic pure rock salt; (**c**) natural pure mudstone; (**d**) synthetic pure mudstone.

From Figure 13a,b, we can see that both the natural pure rock salt and the synthetic pure rock salt have a lattice crystal structure. The crystal lattice of the natural salt rock is larger than that of the synthetic mudstone, and the arrangement of natural pure rock salt is more disordered; this is because, in the process of comminution then remolding, the natural salt rock lattice is shattered and rearranged. From Figure 13c,d, we know that the synthetic mudstone is more closely arranged between particles.

We show the pore size distribution of synthetic pure rock salt, synthetic pure mudstone, natural pure rock salt and natural pure mudstone by mercury intrusion porosimetry (MIP) in Figure 14.

From Figure 14a,b, the intrusion and extrusion of mercury in the natural pure rock salt and the synthetic pure rock salt is mainly controlled by the 10-nm pore size, and the two are in good agreement. From Figure 14c,d, we can see that the intrusion and extrusion of mercury in the natural pure mudstone and the synthetic pure mudstone are mainly controlled by the 20-nm pore size, and the two are in good agreement.

The SEM and the pore size distribution of synthetic specimens and natural specimens are similar, which shows that synthetic material permeability model is a reasonable analogue to the natural specimens.

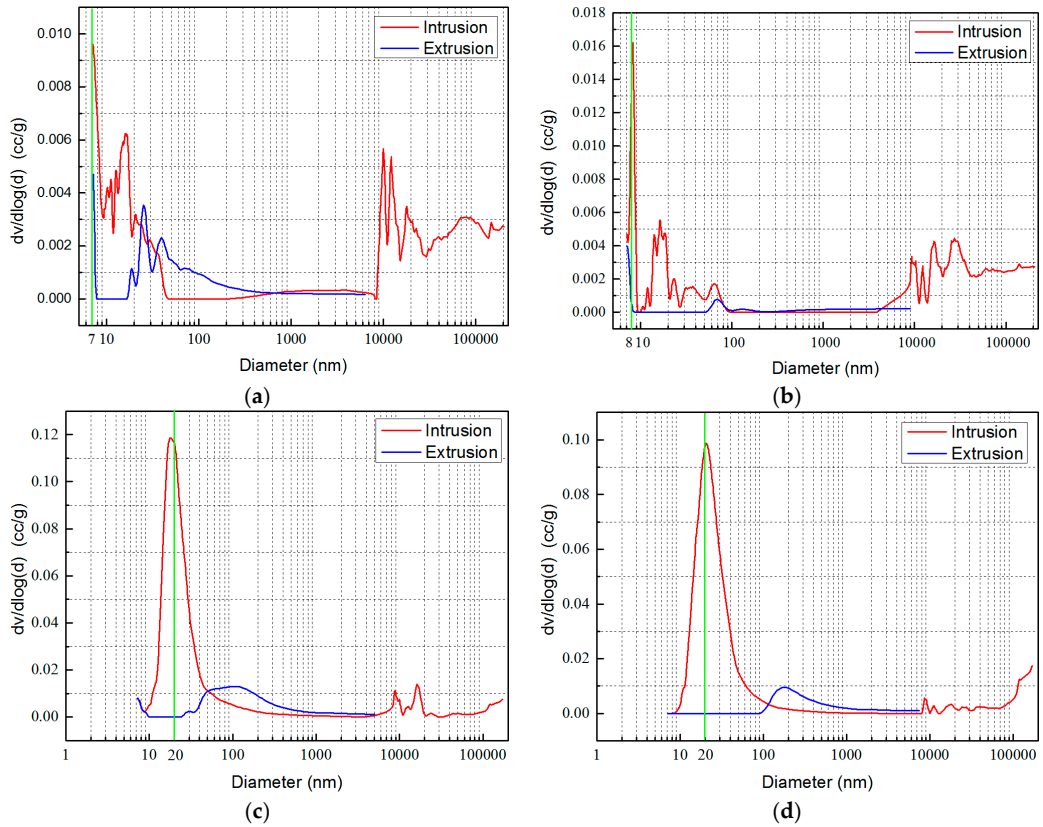

Figure 14. Pore size distribution. (**a**) Natural pure rock salt; (**b**) synthetic pure rock salt; (**c**) natural pure mudstone; (**d**) synthetic pure mudstone.

5.3. The Effect of Porosity on Permeability

As can be seen from Figure 15, the porosity affects the permeability greatly; there is a strong power function between permeability and porosity. The permeability increases with increasing porosity, and when the porosity is less than 10%, the increase is slower, while the permeability increases greatly when the porosity exceeds 10%. This indicates that the porosity has a large effect on the permeability and that the permeability depends on the internal pores and microcracks, as well as their interconnectivity (pore throat size distribution).

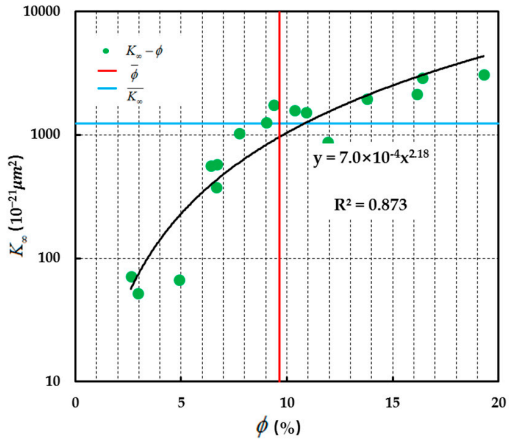

Figure 15. The relationship between K_∞ and ϕ.

5.4. The Influences of Mudstone Content on the Permeability of Specimens

It can be seen from Figure 16 that the Klinkenberg permeability increases with the increase of mudstone content for both kinds of specimens. There is a strong exponential relationship between Klinkenberg permeability and mudstone content of rock salt. We also find that for both kinds of specimens, when the mudstone content is below 40%, the permeability increases only slightly with mudstone content, whereas above this threshold, the permeability increases rapidly with mudstone content. When the mudstone content of rock salt is below 40%, the rock salt particles are closely arranged between each other, while the mudstone particles are relatively less, so the mudstone content has little impact on the Klinkenberg permeability. However, when the mudstone content ranges from 40%–100%, more particles of mudstone embed around rock salt particles, making the connection between the particles of rock salt less dense, so that some pore channels are formed and the pore throat radius is larger. Hence, with the increase of mudstone content, the Klinkenberg permeability increases rapidly when the mudstone content exceeds 40%, and when the mudstone content is 80%, the Klinkenberg permeability is close to the synthetic pure mudstone specimen value.

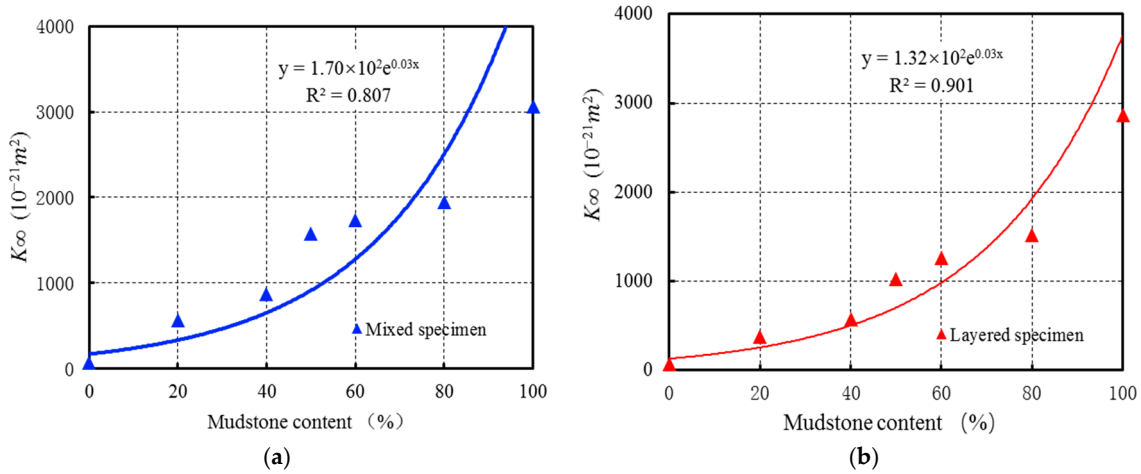

Figure 16. The relationship between K_∞ and mudstone content. (**a**) Mixed specimen; (**b**) layered specimen.

6. Conclusions

(1) During the experiment, it was found that the mudstone is more compressible than rock salt, and the compressibility of rock increased with the increase of porosity.

(2) The pseudo-pressure seepage equation has extensive application value, so the specimen permeability was calculated by the pseudo-pressure method. The Klinkenberg permeability of the synthetic specimens was obtained by curve-fitting. The permeability of synthetic pure rock salt was 6.93×10^{-20} m^2 and its porosity 3.8%, and the permeability of synthetic pure mudstone was 2.97×10^{-18} m^2, with a porosity 17.8%. The test results were close to the natural specimens, and it shows that this synthetic material permeability model is a reasonable analogue of use in engineering.

(3) Comparing permeability test results for the two kinds of synthetic specimens, it was found that the permeability of the mixed specimens was about 40% higher than that of the layered rock salt specimens at the same mudstone content. This suggests that in salt cavern gas storage cases, the layered rock salt is tight at the top and bottom of the cavity. The permeability of the transition zone of rock salt and mudstone around the cavity is higher, and the transition zone would be the permeable channel to be concerned with; although the permeabilities are still very low, and there would also be the beneficial effect of capillary blockage of the brine-filled channels in the field case.

(4) We also found that for both kinds of specimens, there was a strong exponential relationship between Klinkenberg permeability and mudstone content: when the mudstone content is below 40%,

the Klinkenberg permeability increases only slightly with mudstone content, whereas above this threshold, the Klinkenberg permeability increases significantly.

Note: The formation mechanisms of natural rock specimen and synthetic specimen were different. Natural rock was formed in the long-term diagenesis, while the synthetic specimens in this paper were formed in ultra-high pressure. The porosity and permeability of synthetic specimens were similar to the natural specimens, but the natural rock (mudstone/salt) had different pore space structures compared to the synthetic specimens. Therefore, the approach, respectively the outcome (permeability/porosity relationship), can only be a first attempt at investigation.

Acknowledgments: The authors wish to acknowledge the financial support of the National Natural Science Foundation of China (Grant Nos. 51774266, 51404241, 41602328), National Natural Science Foundation of China Innovative Research Team [Grant No. 51621006], and Natural Science Foundation for Innovation Group of Hubei Province, China [Grant No. 2016CFA014]. Moreover, the authors wish to thank the reviewers for constructive comments and suggestions that have helped us improve our manuscript.

Author Contributions: The paper was written by Hongwu Yin under the guidance of Chunhe Yang. The experiment scheme, data analysis and pre-literature research were carried out by Hongling Ma and Xilin Shi. Maurice B. Dusseault deepened the conclusions and did the English editing of the paper. The experiment was carried out by Hongwu Yin under the help of Xiangsheng Chen and Yuhao Zhang.

Conflicts of Interest: The authors declare no conflict of interest.

References

1. Li, Y.P.; Jiang, W.D.; Liu, J.; Chen, J.W.; Yang, C.H. Direct shear tests for layered salt rocks of yunying salt mine in hubei province. *Chin. J. Rock Mech. Eng.* **2007**, *26*, 001767–001772. (In Chinese)
2. Li, Y.P.; Yang, C.H.; Luo, C.W.; Qu, D.A. Study on sealability of underground energy storage in deep salt formation in yunying area, Hubei province. *Chin. J. Rock Mech. Eng.* **2007**, *26*, 2430–2436. (In Chinese)
3. Xu, F.; Yang, C.; Guo, Y.; Wang, T.; Wang, L.; Zhang, P. Effect of confining pressure on the mechanical properties of thermally treated sandstone. *Curr. Sci.* **2017**, *112*, 1101–1106.
4. Liu, W.; Nawaz, M.; Li, Y.P.; Spiers, C.J.; Yang, C.H.; Ma, H.L. Experimental study of permeability of salt rock and its application to deep underground gas storage. *Chin. J. Rock Mech. Eng.* **2014**, *33*, 1953–1961. (In Chinese)
5. Wu, W.; Hou, Z.M.; Yang, C.H. Investigations on permeability of rock salt. *Chin. J. Geotech. Eng.* **2005**, *27*, 746–749. (In Chinese)
6. Zhou, H.W.; He, J.M.; Wu, Z.D. Permeability and meso-structure characteristics of bedded salt rock. *Chin. J. Rock Mech. Eng.* **2009**, *28*, 2068–2073. (In Chinese)
7. Xi, B.P.; Zhao, Y.S.; Zhao, Y.L.; Kang, Z.Q. Investigation on rheodestruction and permeability of surrounding rock for long-term running storage cavern in bedded rock salt. *Rock Soil Mech.* **2008**, *29*, 245–250. (In Chinese)
8. Petrasch, J.; Meier, F.; Friess, H.; Steinfeld, A. Tomography based determination of permeability, Dupuit–Forchheimer coefficient, and interfacial heat transfer coefficient in reticulate porous ceramics. *Int. J. Heat Fluid Flow* **2008**, *29*, 315–326. [CrossRef]
9. Yang, C.H.; Li, Y.P.; Qu, D.A.; Chen, F.; Yin, X.Y. Advances in researches of the mechanical behaviors of bedded salt rocks. *Adv. Mech.* **2008**, *38*, 484–494. (In Chinese)
10. Liu, W.; Li, Y.P.; Yang, C.H.; Ma, H.L.; Liu, J.X.; Wang, B.W.; Huang, X.L. Investigation on permeable characteristics and tightness evaluation of typical interlayers of energy storage caverns in bedded salt rock formations. *Chin. J. Rock Mech. Eng.* **2014**, *33*, 500–506. (In Chinese)
11. Berest, P.; Brouard, B.; Durup, J.G. Tightness Tests in Salt-Cavern Wells. *Oil Gas Sci. Technol.* **2002**, *56*, 451–469. [CrossRef]
12. Cosenza, P.; Ghoreychi, M.; Bazargan-Sabet, B.; Marsily, G.D. In situ rock salt permeability measurement for long term safety assessment of storage. *Int. J. Rock Mech. Min. Sci.* **1999**, *36*, 509–526. [CrossRef]
13. Beauheim, R.L.; Roberts, R.M. Hydrology and hydraulic properties of a bedded evaporite formation. *J. Hydrol.* **2002**, *259*, 66–88. [CrossRef]
14. Popp, T.; Kern, H.; Schulze, O. Evolution of dilatancy and permeability in rock salt during hydrostatic compaction and triaxial deformation. *J. Geophys. Res. Solid Earth* **2001**, *106*, 4061–4078. [CrossRef]

15. Allemandou, X.; Dusseault, M. Healing processes and transient creep of salt rock. *Geotech. Eng. Hard Soils-Soft Rocks.* **1993**, *1*, 3.
16. Stormont, J.C.; Daemen, J.J.K. Laboratory study of gas permeability changes in rock salt during deformation. *Int. J. Rock Mech. Min. Sci. Geomech. Abstr.* **1992**, *29*, 325–342. [CrossRef]
17. Wu, Z.D.; Zhou, H.W.; Ding, J.Y.; Ran, L.N.; Yi, H.Y. Research on permeability testing of rock salt under different permeability pressures. *Chin. J. Rock Mech. Eng.* **2012**, *31*, 3740–3746. (In Chinese)
18. Yan, Q.B.; Chen, M.L.; Wang, J.; Du, Y.; Wang, X.X. Correlation among permeability, porosity and pore throat radius of carbonate reservoirs. *Nat. Gas Ind.* **2015**, *35*, 30–36. (In Chinese)
19. Chen, W.Z.; Tan, X.J.; Wu, G.J.; Yang, J.P. Research on gas seepage law in laminated salt rock gas storage. *Chin. J. Rock Mech. Eng.* **2009**, *28*, 1297–1304. (In Chinese)
20. Zhang, Q.Y.; Liu, D.J.; Jia, C.; Shen, X.; Liu, J.; Duan, K. Development of geomechanical model similitude material for salt rock oil-gas storage medium. *Rock Soil Mech.* **2009**, *30*, 3581–3586. (In Chinese)
21. Ren, S.; Ren, Y.W.; Jiang, D.Y.; Chen, J.; Yang, C.H. Study of synthetic rock salt similar materials for solution mining test. *Chin. J. Rock Mech. Eng.* **2012**, *31*, 3716–3724. (In Chinese)
22. Jiang, D.Y.; Zhang, J.W.; Qu, D.A.; Chen, J.; Yang, C.H. Experimental study on a similar material of rock salt with interlayer. *J. China Coal Soc.* **2013**, *38*, 76–81. (In Chinese)
23. American Petroleum Institute. Practices for Core Analysis. In *SY/T5336–2006. API RP 40–1998 Recommended Practices for Core Analysis*, 2nd ed.; American Petroleum Institute: Washington, DC, USA, 2006.
24. Kong, X.Y. *Advanced Mechanics of Fluid in Porous Media*; Press of University of Science and Technology of China: Hefei, China, 2010. (In Chinese)
25. Hall, H.N. Compressibility of Reservoir Rocks. *J. Pet. Technol.* **1953**, *5*, 17–19. [CrossRef]
26. Li, C.L. The relationship between rock compressibility and porosity. *China Offshore Oil Gas (Geol.)* **2003**, *17*, 355–358. (In Chinese)
27. Liu, H.W. *Advanced Mechanics of Materials*; Higher Education Press: Beijing, China, 1985. (In Chinese)
28. Li, Q.; Gao, S.S.; Liu, H.X.; Ye, L.Y.; Gai, Z.H. Core permeability calculation methods and application scopes. *Nat. Gas Ind.* **2015**, *35*, 68–73. (In Chinese)
29. Klinkenberg, L.J. The Permeability of Porous Media to Liquids and Gases. *Socar Proc.* **1941**, *2*, 200–213. [CrossRef]
30. Scheidegger, A.E. The physics of flow through porous media. *Soil Sci.* **1958**, *86*, 355. [CrossRef]
31. Huang, J.Z.; Feng, J.M. Simplification of conventional methods for obtaining permeability. *Pet. Explor. Dev.* **1994**, *21*, 54–58. (In Chinese)
32. Gueguen, Y.; Palciauskas, V.; Jeanloz, R. Introduction to the Physics of Rocks. *Phys. Today* **1995**, *48*. [CrossRef]
33. Ge, J.L. *The Modern Mechanics of Fluids Flow in Oil Reservoir*; Petroleum Industry Press: Beijing, China, 2003. (In Chinese)
34. American Petroleum Institute. *Orifice Metering of Natural Gas and Other Related Hydrocarbon Fluids—Concentric, Square-Edged Orifice Meters—Part 1: General Equations and Uncertainty Guidelines*; API MPM CH14.3.1 Ed. 4; American Petroleum Institute: Washington, DC, USA, 2012.
35. Yang, C.H.; Li, Y.P.; Chen, F. *Mechanics Theory and Engineering of Bedded Rock Salt*; Science Press: Beijing, China, 2009. (In Chinese)